

Percolation and Colossal Magnetoresistance in Eu-based Hexaborides

G.A. Wigger, C. Beeli, E. Felder, and H. R. Ott

Laboratorium für Festkörperphysik, ETH-Hönggerberg, CH-8093 Zürich, Switzerland

A.D. Bianchi* and Z. Fisk

National High Magnetic Field Laboratory, Florida State University, Tallahassee, Florida 32306

(Dated: February 2, 2008)

Upon substituting Ca for Eu in the local-moment ferromagnet EuB_6 , the Curie temperature T_C decreases substantially with increasing dilution of the magnetic sublattice and is completely suppressed for $x \leq 0.3$. The Ca substitution leads to significant changes of the electronic properties across the $\text{Eu}_x\text{Ca}_{1-x}\text{B}_6$ series. Electron microscopy data for $x \approx 0.27$ indicate a phase separation into Eu- and Ca-rich clusters of 5 to 10 nm diameter, leading to percolation-type phenomena in the electrical transport properties. The related critical concentration x_p is approximately 0.3. For $x \approx 0.27$, we observe colossal negative magnetoresistance effects at low temperatures, similar in magnitude as those reported for manganese oxides.

PACS numbers: 72.15.Gd, 75.30.Kz, 75.47.Gk

Strong variations of the electrical resistivity ρ by external magnetic fields may be achieved either in specially tailored thin-film heterostructures, leading to so called giant magnetoresistance [1], or in manganese oxides which exhibit metal/insulator transitions and concomitant magnetic ordering phenomena, leading to colossal magnetoresistance effects [2]. Giant magnetoresistance is related to the spin-dependent scattering of conduction electrons between magnetically ordered layers which is strongly affected by external fields [3]. Colossal magnetoresistance is traced back to a strong coupling of the electronic subsystem to the lattice, leading to polaron formation [4]. The onset of ferromagnetic order, favored by applying external fields, induces a transition to a metallic, i.e., low resistive state.

Large magnetoresistance effects are also known to occur in some Eu-based chalcogenides [5] and in EuB_6 [6]. Also here, ferromagnetism favors metallicity, both by enhancing the number of itinerant charge carriers and by reducing the spin disorder scattering [7]. Again, increasing magnetic fields help to enhance the electrical conductivity of the respective materials.

In this work, we present and discuss a set of electrical transport data for materials of the series $\text{Eu}_x\text{Ca}_{1-x}\text{B}_6$ and demonstrate that they are strongly influenced by a phase separation between nanoscopically small Eu- and Ca-rich regions. This phenomenon leads to percolation effects in both the onset of magnetic order and the electronic transport. For x close to $x_p = 0.31$, the three dimensional site percolation limit for a simple cubic lattice [8, 9, 10], we observe extremely large negative magnetoresistance effects.

Single-crystalline samples of $\text{Eu}_x\text{Ca}_{1-x}\text{B}_6$ were grown in a flux of 99.999% pure Al, using the starting elements Eu, Ca and B with purities of 99.95%, 99.987% and 99.99%, respectively. Measurements of the magnetization were made with a commercial SQUID magnetome-

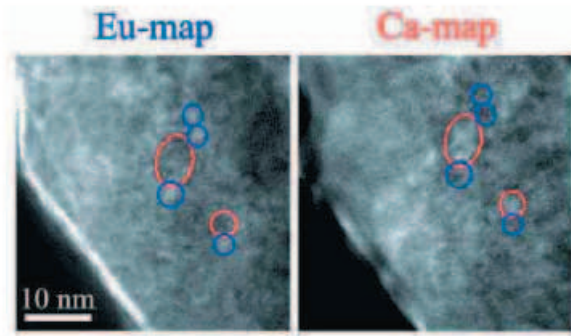


FIG. 1: (Color in online edition) EFTEM images for $x \sim 0.27$. In the left (right) panel, the energy window was chosen such that the electrons scatter inelastically off the Eu- (Ca-) ions. The red (blue) rings mark regions rich in Ca (Eu). Bright (dark) regions indicate a high (low) intensity of scattered electrons

ter. In order to avoid the influence of possible magnetic impurities at the surface, the samples were etched for a short time in strongly diluted nitric acid. High resolution transmission electron microscopy (HRTEM) investigations were made with a FEI Technai F30 instrument, equipped with a field emission electron gun and an energy filter from Gatan Inc. The filter employs an electron energy loss spectrometer (EELS) to select a particular energy window for the inelastically scattered electrons to form the image. The chemical maps shown in Fig.(1) were recorded with the so-called three-window technique. Selected area electron diffraction patterns and HRTEM images, which are both not shown because of space restrictions, reveal the high perfection of the atomic arrangements in the crystals, also for low values of x . However, energy-filtered TEM images reveal a phase separation resulting in Eu- and Ca-rich regions. An example

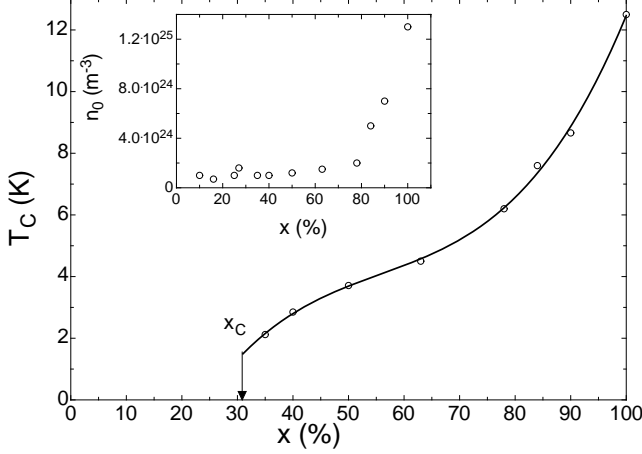


FIG. 2: T_C obtained from magnetization, specific heat and resistivity data. The solid line is to guide the eye. The critical value x_C represents the limit for the site percolation in a cubic 3D lattice. The inset displays the itinerant electron density $n_0(x)$, which is approximately constant between 30 and 70 K for all values of x .

is shown in Fig.(1) for $x = 0.27$. Two patches relatively rich in Ca are marked by red rings, several other patches relatively rich in Eu are emphasized by blue rings. The comparison of the two maps reveals that a relative richness in one element is correlated with a relative deficiency in the other. Analogue Boron maps confirm a constant distribution of the anion element. The typical diameter of the clusters is between 5 and 10 nm. In view of the different concentrations of charge carriers in the different regions (see inset of Fig.(2)), the maps shown in Fig.(1) may also be taken as evidence for an electronic phase separation and hence the formation of regions with different electrical conductivities.

The resistivities and the Hall voltages were measured using a standard low-frequency a.c. four-contact technique in longitudinal and transversal configuration, respectively. The covered temperature and magnetic field ranges were between 0.35 and 300 K, and 0 and 7 Tesla, respectively.

In Fig.(2) we present the x dependence of the Curie temperature $T_C(x)$ as established by measurements of the specific heat $C_p(T)$ and the electrical resistivity $\rho(T)$ in zero magnetic field, as well as by Arrott-plot analyses of the magnetization $M(T, H)$. T_C decreases monotonously but non linearly with decreasing x and vanishes at $x \sim 0.3$. The non-linear decrease of $T_C(x)$ most likely reflects the formation of Eu- and Ca-rich regions, whereby x merely represents an average concentration of Eu ions. For $x \leq 0.3$, i.e., below the percolation limit, the ground state exhibits spin-glass type features [11].

In the following we argue that the phase separation is also reflected in the electronic transport properties across

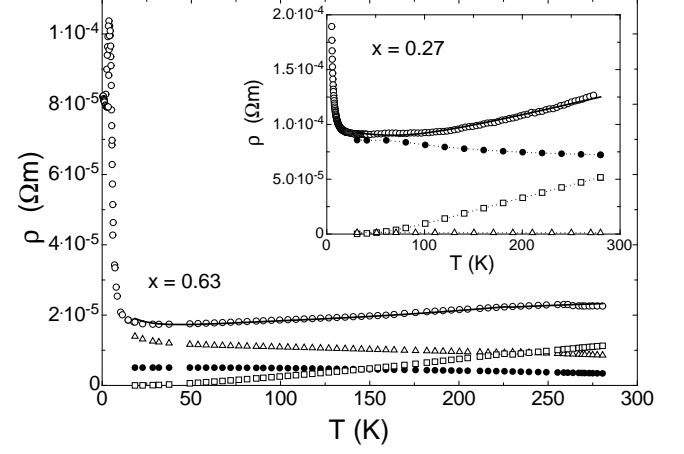


FIG. 3: Separation of $\rho(T)$ (open circles) for material with $x = 0.63$ into spin-disorder (triangles), electron-phonon (squares) and defect-induced resistivity (full circles). The solid line is the result of our calculation described in the text. The inset shows the same for $x = 0.27$. Here, the dotted lines are to guide the eye.

the series. As described in detail before [12, 13], the total electrical resistivity ρ of these materials is due to different contributions. In our case we consider

$$\rho = \rho_{sd} + \rho_{e-ph} + \rho_d \quad , \quad (1)$$

where ρ_{sd} , ρ_{e-ph} and ρ_d represent the spin-disorder, the electron-phonon and the defect scattering, respectively.

Because in these hexaborides, the concentration of conduction electrons is temperature dependent, all three contributions to $\rho(T)$ vary with temperature, in particular also ρ_d . It is ρ_d which is mainly affected by the phase separation and therefore is expected to reflect the influence of percolation effects most significantly.

The spin disorder scattering is taken into account by [14, 15]

$$\rho_{sd} = \frac{1}{4\pi^{1/3}} \frac{Nm^*}{\hbar^3 e^2} \left(\frac{J}{N} \right)^2 xS(xS+1) \frac{T}{T - T_C} n^{-2/3} \quad , \quad (2)$$

with J as the effective exchange interaction parameter, N as the number of cations per unit volume, m^* as the effective mass and n as the concentration of the conduction electrons. For the scattering of electrons on phonons, we used the same model approach that was successful in previously published analyses of the electrical resistivities of LaB_6 [12] and EuB_6 [13], where the phonon spectrum was approximated by a Debye type spectrum and two superimposed Einstein modes. The latter modes model the motion of Eu and Ca ions inside the respective Boron cages. The Debye temperature was taken as 1160 K, as

previously reported [12, 13]. The best fits were obtained with Einstein temperatures of 168 K and 373 K for the Eu and the Ca mode, respectively. The activation of mobile charge carriers out of defect states, implied by results of Hall voltage measurements [11, 13], was considered by setting

$$n(x, T) = n_0(x) + \Delta n(x) \cdot e^{-E_{ex}(x)/k_B T} , \quad (3)$$

where $n_0(x)$ represents the constant mobile-carrier densities in the range $30 \text{ K} \leq T \leq 70 \text{ K}$, shown in the inset of Fig.(2). The excitation energy $E_{ex}(x)$ is the energy of defect states with respect to the Fermi energy. The relaxation rate for the defect scattering, assumed to be temperature independent, was evaluated from $\rho_d = \rho - \rho_{sd} - \rho_{e-ph}$ and $n_0(x)$.

The temperature dependences of the individual contributions, adding up to the total $\rho(T)$ of material with $x = 0.63$ and 0.27 , is shown in Fig.(3). The calculated solid lines are in remarkably good agreement with experiment. In order to emphasize the effect of percolation, $\rho_d(x)$ was scaled to a charge carrier concentration of $1.3 \cdot 10^{25} \text{ m}^{-3}$, the value of $n_0(x = 1)$. From fits to the experimental data for $\rho(T)$ for other values of x , the scaled values of $\rho_d(x)$ were evaluated and plotted in the main frame of Fig.(4). The usual Nordheim-Kurnakov relation [16] for a two component system

$$\rho_d(x) \sim x(1 - x) \quad (4)$$

is not even qualitatively obeyed. Instead a tendency to divergence at $x \sim 0.33$, close to the above mentioned site percolation limit for a simple cubic system of $x_p = 0.31$ is observed. A percolation dominated resistivity is expected to be described by

$$\rho_d = \rho'_d(x - x_p)^{-t} + \rho_\infty , \quad (5)$$

with $1.5 \leq t \leq 1.6$ [17, 18, 19]. In our case, $\rho_\infty \approx 4.2 \cdot 10^{-7} \Omega \text{m}$. A first attempt to fit the data for $x > 0.35$ and assuming $x_p = 0.31$, resulted in $t = 1.12 \pm 0.05$, distinctly smaller than expected. The corresponding fit is represented by the dotted line in Fig.(4). A forced fit with $t = 1.5$, shown as the broken line in Fig.(4), results in $x_p = 0.29$. Although no perfect agreement between theoretical expectations and experiment is achieved in this way, the qualitative behaviour of $\rho_d(x)$ strongly suggests that percolation plays a dominant role. This is supported by the inset of Fig.(4), where $\rho_d - \rho_\infty$ is plotted versus $(x - x_p)$ on double logarithmic scales. The solid line represents a power law variation with $t = 1.5$.

Considering that both the Eu-, as well as the Ca-rich regions are conducting, it seems reasonable to inspect whether a phenomenological interpretation of the effective media theory due to Bruggeman [20], treating two

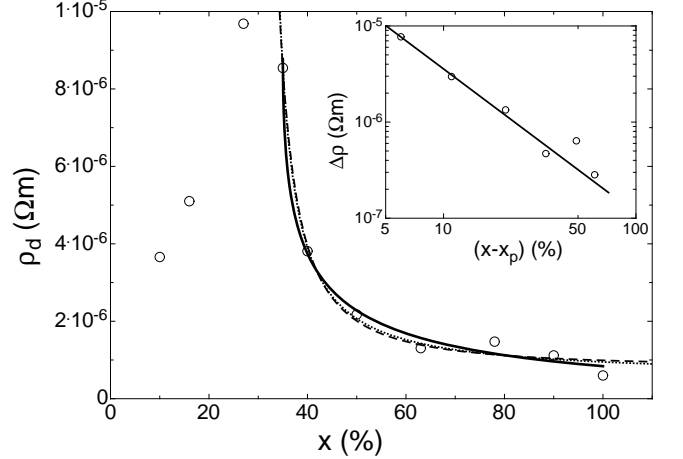


FIG. 4: $\rho_d(x)$. The dotted and the broken line describe fits according to eq. 5 with $t = 1.2$ and 1.5 , respectively. The solid line is a solution to eq. 7. The inset shows $\Delta\rho = \rho_d - \rho_\infty$ vs. $x - x_p$ on a log-log scale. This verifies the power law with exponent 1.5 .

or more constituents with different conductivities σ_i and different volume fractions f_i , is more appropriate for our case. This approach, due to McLachlan [21], yielded very good agreement with experimental results by interpolating between the symmetric and the antisymmetric solution of the Bruggeman model. The scheme retains Bruggeman's solution in the limiting cases with the correct values for x_p and t . For our purpose we consider two components; Eu-rich regions with a volume fraction f and a high conductivity σ_h , and Ca-rich regions with a volume fraction $(1 - f)$ and a low conductivity σ_l . Volume fractions can be converted to atomic fractions by using

$$f = \frac{R \cdot x}{R \cdot x + (1 - x)} , \quad (6)$$

where x is the atomic bond or site fraction and R is the effective ratio of the two volumes. In our case, volume effects are negligible because the lattice parameter changes only by about 1% across the entire series and we may set $f = x$ and $f_c = x_p$. The conductivity of the effective medium is found by solving [21]

$$\frac{f(\Sigma_h - \Sigma_m)}{\Sigma_h + \frac{f_c}{1-f_c}\Sigma_m} + \frac{(1-f)(\Sigma_l - \Sigma_m)}{\Sigma_l + \frac{f_c}{1-f_c}\Sigma_m} = 0 , \quad (7)$$

where Σ_m is the scaled conductivity of the effective medium and $\Sigma_i = \sigma_i^t = \rho_i^{-t}$ for $i = h, l$ and m . Based on this model we attempted to fit the ρ_d data by assuming $t = 1.5$. The best result, represented by the solid line in Fig.(4), yielded $\rho_h = 8.7 \cdot 10^{-7} \Omega \text{m}$ and $\rho_l = 2.6 \cdot 10^{-6} \Omega \text{m}$, respectively. These values are close to $\rho_d(x = 1)$

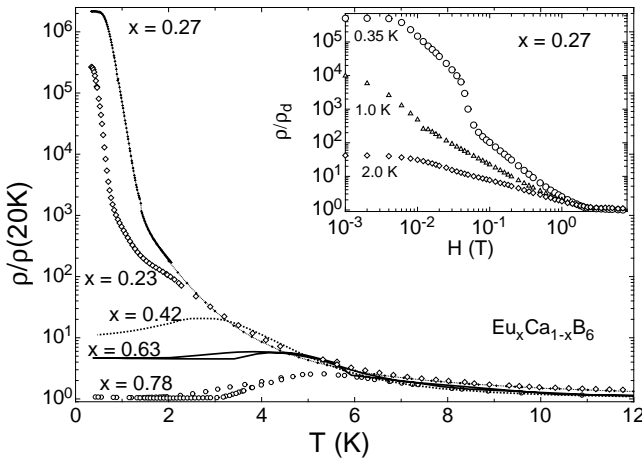


FIG. 5: $\rho/\rho(20K)$ for $x = 0.23, 0.27, 0.42, 0.63, 0.78$. The inset shows $\rho(H)/\rho_d$ for $x = 0.27$ at 0.35, 1.0 and 2.0 K.

and, particularly rewarding, $\rho_d(x = 0)$, respectively. The percolation limit turns out to be $x_p \sim 0.33$, slightly higher than the mentioned site percolation limit.

For material with x close to but below x_p , we observe remarkable magnetoresistance effects at very low temperatures. In Fig.(5), $\rho(T)$ in zero external magnetic field is shown for specimens with different values of x . The materials with $x = 0.27$ and 0.23 do not exhibit long range magnetic order at low temperatures. Instead, spin-freezing type phenomena as evidenced by the results of specific heat and a.c. susceptibility measurements [11] were observed. It is remarkable, that $\rho(T)$ continues to increase dramatically below the spin-freezing transitions at about 2 K. The inset of Fig.(5) demonstrates that the strong enhancement of ρ at low temperatures can be eliminated by magnetic fields of moderate strength. A more detailed discussion of these $\rho(H)$ data will be published elsewhere. The $\rho(T, 0)$ curves are qualitatively similar to those that were previously reported for manganese oxides of the type $(La_{5/8-y}Pr_y)Ca_{3/8}MnO_3$ [22]. It was claimed that for these materials, intrinsic inhomogeneities due to phase separation are responsible for colossal magnetoresistance effects. A theoretical interpretation of those data, calculating the inverse conductivity for 3D percolative systems [23], resulted in $\rho(T, 0)$ curves of qualitatively the same shape as those shown in Fig.(5).

We intended to demonstrate that electronic phase separation, related percolation and colossal magnetoresistance phenomena, previously reported for selected oxide compounds [22], may also be found in systems as simple as the cubic hexaborides. Although we cannot yet provide a convincing link between the different phenomena in our case, ours and previous results indicate a favorable route for future research efforts in relation with colossal

magnetoresistance effects.

Stimulating discussions with R. Monnier are gratefully acknowledged. This work has benefitted from partial financial support of the Schweizerische Nationalfonds zur Förderung der wissenschaftlichen Forschung and the US-NSF grant DMR-0203214.

* Present address: Hochfeldlabor Dresden Forschungszentrum Rossendorf, Postfach 51 01 19, 01314, Dresden Germany

- [1] P. Grünberg, R. Schreiber, Y. Pang, M.B. Brodsky, and H. Sowers, Phys. Rev. Lett. **57**, 2442 (1986); M.N. Baibich, J.M. Broto, A. Fert, F. Nguyen Van Dau, and F. Petroff, P. Eitenne, G. Creuzet, A. Friederich, and J. Chazelas, Phys. Rev. Lett. **61**, 2472 (1988)
- [2] S. Jin, T.H. Tiefel, M. McCormack, R.A. Fastnacht, R. Ramesh, L.H. Chen, Science **264**, 413 (1994)
- [3] J.M. De Teresa, A. Barthélémy, A. Fert, J.P. Contour, F. Montaigne, P. Seneor, Science **286**, 5349 (1999)
- [4] J.F. Lawler, J.M.D. Coey, J. M. M. Mat. **140**, 2049 (1995); H.Y. Hwang, S-W. Cheong, P.G. Radaelli, M. Marezio, and B. Batlogg, Phys. Rev. Letters **75**, 914 (1995).
- [5] T. Kasuya, A. Yanase, Rev. Mod. Phys **40**, 684 (1968).
- [6] R. Bachmann, K.N. Lee, T.H. Geballe and A. Menth, J. Appl. Phys. **41**, 1431 (1970).
- [7] L. Degiorgi, E. Felder, H.R. Ott, J.L. Sarrao, and Z. Fisk, Phys. Rev. Lett. **79**, 5134 (1997).
- [8] S. Kirkpatrick, Solid State Comm. **12**, 1279 (1973).
- [9] B.I. Shklovskii and A.L. Efros, Sov. Phys.-Usp. **18**, 845 (1975).
- [10] B.I. Shklovskii, A.L. Efros, *Electronic Properties of Doped Semiconductors*, Springer (1984)
- [11] G.A. Wigger et al., unpublished.
- [12] D. Mandrus, B. C. Sales and R. Jin, Phys. Rev. B**64**, 12302 (2001).
- [13] G.A. Wigger, R. Monnier, H.R. Ott, D.P. Young and Z. Fisk, cond-mat/0309412.
- [14] K.N.R. Taylor and M.I. Darby, *Physics of Rare Earth Solids* Chapman and Hall LTD, London (1972).
- [15] C. Haas, Phys. Rev. **168**, 531 (1968).
- [16] J.M. Ziman, *Electrons and Phonons*, Clarendon, Oxford (1960).
- [17] S. Kirkpatrick, Rev. Mod. Phys. **45**, 574 (1973).
- [18] A.S. Skal, B.I. Shklovskii, A.L. Efros, Fiz. Tverd. Tela **17**, 506 (1975).
- [19] A.G. Dunn, J.W. Essam, J.M. Loveluck, J. Phys. C.: Solid State **8**, 743 (1975).
- [20] D.A.G. Bruggeman, Z. Phys. **37**, 906 (1936), Ann. Phys. **24**, 665 (1935) and Ann. Phys. **29**, 160 (1937).
- [21] D.S. McLachlan, J. Phys. C: Solid State Phys. **19**, 1339 (1986).
- [22] M. Uehara, S. Mori, C.H. Chen and S-W. Cheong, Nature **399**, 560 (1999).
- [23] M. Mayr, A. Moreo, J.A. Vergés, J. Arispe, A. Feiguin and E. Dagotto, Phys. Rev. Letters **86**, 135 (2001).